

# Load Modulation for Backscatter Communication: Channel Capacity and Capacity-Approaching Finite Constellations

Gregor Dumphart, Johannes Sager, Armin Wittneben

## Abstract

In backscatter communication (BC), a passive tag transmits information by just affecting an external electromagnetic field through load modulation. Thereby, the feed current of the excited tag antenna is modulated by adapting the passive termination load. This paper studies the achievable information rates with a freely adaptable passive load. As a prerequisite, we unify monostatic, bistatic, and ambient BC with circuit-based system modeling. A crucial insight is that channel capacity is described by existing results on peak-power-limited quadrature Gaussian channels, because the steady-state tag current phasor lies on a disk. Consequently, we derive the channel capacity in the case of an unmodulated external field, for a general passive or purely reactive or resistive tag load. We find that modulating both resistance and reactance is crucial for high rates. We discuss the capacity-achieving load statistics, the rate asymptotics, and the capacity of ambient BC in important special cases.

Furthermore, we propose a capacity-approaching finite constellation design: a tailored amplitude-and-phase-shift keying on the reflection coefficient. We also demonstrate high rates for very simple loads of just a few switched resistors and capacitors. Finally, we investigate the rate loss from a value-range-constrained load, which is found to be small for moderate constraints.

## Index Terms

backscatter communication, load modulation, channel capacity, ambient backscatter, RFID

This article was presented in part at the IEEE Wireless Communications and Networking Conference (WCNC), Austin TX, USA, April 2022 [1]. (*Corresponding author: Gregor Dumphart*)

The authors are with the Wireless Communications Group, D-ITET, ETH Zurich, Zürich, 8092 Switzerland, e-mail: dumphart@nari.ee.ethz.ch, sagerj@student.ethz.ch, wittneben@nari.ee.ethz.ch.

This work has been submitted to the IEEE for possible publication. Copyright may be transferred without notice.

## I. INTRODUCTION

Backscatter communication (BC) allows a simple passive tag to transmit data with essentially zero transmit power and no transmit amplifier. Instead, the tag scatters a preexisting external electromagnetic field in an adaptive fashion, in order to modulate data onto this field. The external field can stem from a dedicated unmodulated source or a modulated ambient source [2], [3]. The receiver decodes the data after detecting the changes in the field. BC found widespread use in smart cards and radio-frequency identification (RFID) [4], [5] and is a promising approach to ultra-low-energy communication in wireless sensor networks and the Internet of Things (IoT) [2], [3], [6], [7]. The different basic setups are illustrated in Fig. 1. Promising BC systems that utilize ambient OFDM signals (e.g., commodity Wi-Fi signals) have been presented in [7]–[10]. Other exciting BC applications are given in [11]–[13].

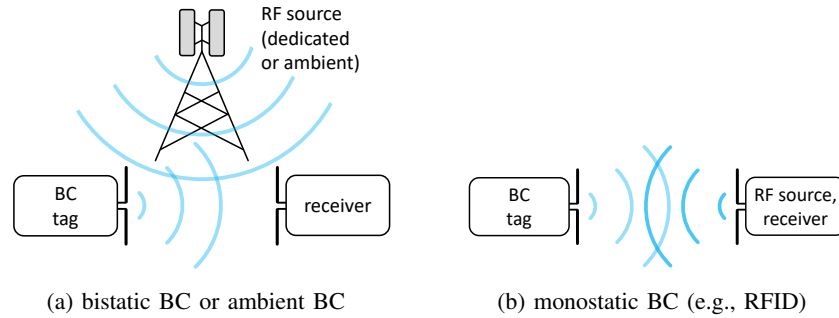


Fig. 1. Different basic setups in backscatter communication. Analogous illustrations were given in [2], [14] among others.

In BC, the tag antenna is excited by an external field and terminated by a passive load. The tag antenna feed current is modulated via load modulation [4], [5] whereby the load is adapted at a chosen symbol rate. For example, switching between a resonant load and an open circuit results in binary amplitude-shift keying for the current. Such 2-ASK modulation has been used in [7]. The data-rate requirements of many IoT applications have however incentivized modulation schemes beyond binary [2, Tab. III] such as quadrature phase-shift keying (4-PSK) in [7], [8] and 16-ary quadrature amplitude modulation (16-QAM) in [15]. It is unclear how well-suited these constellations are to the physical constraints of passive tags. Furthermore, the idea to increase the information rate by ever-increasing constellation sizes will inevitably stagnate: for a very large constellation, the receiver can't reliably distinguish neighboring symbols in the noise, which must be countered with increased redundancy in the employed error-correcting code to ensure reliable decoding. This trade-off caps the information rate and is described in the most general

form by Shannon's channel coding theorem and the notion of channel capacity [16], [17, Cpt. 7]. However, no existing theorem or formula specifically describes the channel capacity of a given BC link. The related question of the capacity-achieving load modulation scheme thus remains unresolved. The answer promises valuable design criteria for high-data-rate BC systems and is also a stepping stone towards optimal ambient backscatter communication.

*Contribution:* This paper presents the channel capacity solution of backscatter load modulation in the general case of a freely adaptable passive load (i.e. no specific constellation is assumed) for monostatic and bistatic links with a single tag, an unmodulated field source, and no antenna arrays. More specifically, the presented core contributions are:

- As a prerequisite, we develop a circuit-based system model that unifies load-modulation links for monostatic BC (MoBC), bistatic BC (BiBC), and ambient BC (AmBC).
- Based on an analysis of the tag-side physical constraints, we apply existing information theory on peak-power-limited quadrature Gaussian channels to solve the channel capacity problem for a general passive load.
- We state the channel capacity also for the special cases where the load is purely reactive or purely resistive.
- We characterize the capacity-achieving load distribution in terms of reflection coefficient and impedance.
- The rate results are discussed by means of bounds and asymptotes. We find that restricting the load to be purely reactive or resistive causes a capacity pre-log factor of  $\frac{1}{2}$ .

Furthermore, we present the following complementary contributions of high technical relevance:

- We show that the results can describe the channel capacity of AmBC in important special cases.
- We present an amplitude and phase-shift keying (APSK) constellation design that allows to approach capacity.
- We show that high rates are possible even with simple load circuits of a few switched resistors and capacitors.
- We characterize how the rate decreases due to an adaptive load with limited dynamic range.

This paper does not consider aspects of tag power consumption, energy harvesting, channel models, or multiple access.

*Related Work:* An important resource on load modulation is the book by Finkenzeller [5]. The research literature contains a limited number of information-theoretic investigations on BC

and load modulation. The simpler case of an unmodulated field source has received particularly little attention. A few works address signal detection in terms of error probabilities and optimal decision thresholds in BC [3], [18], [19] and specifically RFID [20], [21]. The focus of [20] is on the effect of the propagation environment on the Euclidean symbol distances and the resulting bit error rate with PSK and ASK. Zhao et al. [18] calculated the channel capacity of binary load modulation with thresholding in AmBC for various cases of the ambient signal modulation. Kim and Kim [10] studied the maximization of AmBC network capacity in terms of redundancy and modulation (for 2-PSK, 4-PSK, and 16-QAM alphabets) in a WiFi OFDM setting. Hoang et al. [22] contrasted AmBC with the harvest-then-transmit approach.

A rich work on BC information theory has been published by Darsena et al. [14]. They noted the important role of the load reflection coefficient  $\Gamma \in \mathbb{C}$ ,  $|\Gamma| \leq 1$ , and that it implies an instantaneous amplitude constraint. This was invoked in the capacity analysis, albeit based on the results of Smith 1971 [23] which apply only to real-valued but not to complex-valued Gaussian channels (as clarified in much detail in [24]).

Duan et al. [25] studied the achievable rate of AmBC with a MIMO legacy system and a multi-antenna tag that uses polyphase-coding modulation and leaves the amplitude unmodulated. A comparison to Gaussian signaling hints that modulating also the amplitude promises significant rate gains at high SNR.

*Paper Structure:* Sec. II develops the employed system model and analyzes the tag-side constraints. Sec. III presents the channel capacity result, the associated distribution, and the discussion based on bounds and asymptotes. Sec. IV explains implications for the channel capacity of AmBC. Sec. V addresses practical modulation aspects such as the design of suitable constellations and load circuits. Sec. VI concludes the paper.

*Notation:* For a random variable  $\mathbf{x}$  (written boldface italic), we denote a realization as  $x$  (lightface italic), the probability density function (PDF) as  $f_{\mathbf{x}}(x)$ , and the expected value as  $\mathbb{E}[\mathbf{x}]$ . We use the imaginary unit  $j$  with  $j^2 = -1$  and the Euler number  $e$ . Random vectors occur only briefly in Sec. IV and are denoted like  $\vec{\mathbf{x}}$ . Matrices do not occur. All information quantities are in unit bit unless explicitly stated otherwise. We refer to modulation schemes in the style 2-PSK and 4-PSK instead of BPSK and QPSK.

## II. SYSTEM MODELING

Before studying the information theory of load-modulated BC, we first develop an adequate system model for tag-to-receiver links, based on the circuit model in Fig. 2. It encapsulates both setups from Fig. 1a and 1b and is inspired by the circuit models in [5, Sec. 4.1]. The

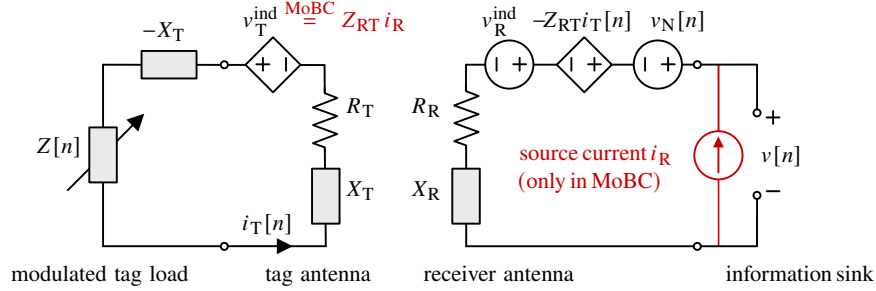


Fig. 2. Unified circuit description of BC links. A passive load-modulation tag (left) transmits to a coupled information receiver (right). The voltage measurement  $v[n]$  is the starting point for the receive signal processing. In monostatic BC (red), the receiver is also the power source (via the source current  $i_R$ ).

left-hand circuit models the passive tag. Its adaptive load impedance  $Z[n] \in \mathbb{C}$  must fulfill  $\text{Re}(Z[n]) \geq 0 \forall n$  because the load is passive [26, Sec. 4.1]. Thereby  $n \in \mathbb{Z}$  is the symbol time index. The given tag-side induced voltage, represented by the phasor  $v_T^{\text{ind}} \in \mathbb{C}$ , is the crucial cause for any electrical activity at the tag. The tag current phasor  $i_T[n] \in \mathbb{C}$  is altered by  $Z[n]$ . The tag-antenna impedance  $R_T + jX_T$  has its reactance  $X_T$  purposefully canceled by the serial reactance  $-X_T$  in order to establish a near-resonant state. The right-hand circuit is an information receiver that measures a voltage phasor  $v[n] \in \mathbb{C}$ . The measurement is impaired by the noise voltage  $v_N[n] \in \mathbb{C}$  and the interfering induced voltage  $v_R^{\text{ind}}$ . The tag and receiver antennas are coupled via the mutual impedance  $Z_{RT} \in \mathbb{C}$ , which encapsulates all aspects of the propagation channel.

For the ambient and bistatic cases, the circuit assumes that the voltages  $v_T^{\text{ind}}, v_R^{\text{ind}} \in \mathbb{C}$  are induced by an electromagnetic field from some external radio-frequency (RF) source (not shown in Fig. 2). These cases differ in one aspect: AmBC assumes randomly modulated  $v_T^{\text{ind}}, v_R^{\text{ind}}$  while BiBC assumes constant  $v_T^{\text{ind}}, v_R^{\text{ind}}$  because of a dedicated unmodulated RF source [2].

Monostatic BC does not assume any external source. Instead, the information receiver is also the system's power source (e.g., an RFID reader) and the crucial tag-side induced voltage is  $v_T^{\text{ind}} = Z_{RT} i_R$  as a consequence of the source current  $i_R$ . A prominent example of MoBC is

inductive RFID, where  $X_T, X_R, Z_{RT}$  are determined by inductances and where  $-X_T$  is realized by a resonance capacitor [5].

For the tag antenna we assume the minimum-scattering property [27] which asserts that the electromagnetic field is left unaltered by an open-circuited tag ( $Z = \infty$ ). We assume that  $Z[n]$  is piecewise constant over time and that it changes instantaneously at the symbol switching instants. We neglect any signal transients which result for  $i_T$  and  $v$ . This is a meaningful assumption if the symbol duration is significantly larger than the circuits' time constants. Our previous work [28, Appendix E] showed that transients do not cause significant deterioration for the receive processing of load-modulated signals. When anticipated, they can actually improve the SNR.

We characterize the electrical state of the tag load with the following complex-valued quantities:

*load impedance (unit ohm):*

$$Z = R_T \cdot z = R_T \frac{1 + \Gamma}{1 - \Gamma}, \quad \text{Re}(Z) \geq 0, \quad (1)$$

*normalized load impedance:*

$$z = \frac{Z}{R_T} = \frac{1 + \Gamma}{1 - \Gamma}, \quad \text{Re}(z) \geq 0, \quad (2)$$

*load reflection coefficient:*

$$\Gamma = \frac{Z - R_T}{Z + R_T} = \frac{z - 1}{z + 1}, \quad |\Gamma| \leq 1. \quad (3)$$

The reference impedance is set to the tag-antenna resistance  $R_T$  (not to the typical  $50\Omega$ ). The Möbius transformation  $\Gamma = \frac{z-1}{z+1}$  in (3) is a bijective map from the right half-plane  $\text{Re}(z) \geq 0$  to the unit disk  $|\Gamma| \leq 1$ . It underlies the well-known Smith chart [26, Eq. (2.53)].

The tag current resulting from the load state is

$$i_T[n] = \frac{v_T^{\text{ind}}}{R_T + Z[n]} = \frac{2 \cdot i_0}{1 + z[n]} = (1 - \Gamma[n]) i_0. \quad (4)$$

Thereby,  $i_0$  is the tag current with a matched load ( $z = 1$ ),

$$i_0 := \frac{v_T^{\text{ind}}}{2 \cdot R_T}. \quad (5)$$

The formula  $i_T[n] = (1 - \Gamma[n]) i_0$  together with  $|\Gamma[n]| \leq 1$  characterizes the transmit currents that can be realized by a passive tag. Specifically, the set of realizable transmit currents  $i_T \in \mathbb{C}$  is given by a disk  $|i_T[n] - i_0| \leq |i_0|$  with center  $i_0 \in \mathbb{C}$  and radius  $|i_0|$ . Analogous observations have been made in [5, Sec. 4.1] and [14].

The achievable information rate of the link is determined by the relationship between  $i_T[n]$  and  $v[n]$ . It would be confusing to apply information theory directly to those quantities, because of the intricate constraint on  $i_T[n]$  and the case-specific receiver differences. For this reason, we introduce two signal transformations that simplify the mathematics while leaving the mutual information unaltered. As a preceding step, we express the receive voltage:

$$v[n] = -Z_{RT} i_T[n] + v_N[n] + \begin{cases} (R_R + jX_R)i_R & \text{MoBC} \\ v_R^{\text{ind}} & \text{BiBC} \\ v_R^{\text{ind}}[n] & \text{AmBC} \end{cases} . \quad (6)$$

To unify these cases within the same system model, we consider a specific receive-side signal compensation:

$$v_{\text{diff}}[n] := v[n] - v|_{Z_{RT}i_T=0, v_N=0} \quad (7)$$

$$= -Z_{RT} i_T[n] + v_N[n] . \quad (8)$$

The processing rule (7) will require a high-resolution receiver with precise a-priori calibration in the absence of the tag (such that  $Z_{RT}i_T = 0$ ). MoBC faces the challenge of canceling the strong self-interference voltage at the receiver [5, Sec. 6.2.4], [6]. In BiBC, the direct-path interference  $v_R^{\text{ind}}$  is constant and must be estimated precisely in order to cancel it. In AmBC,  $v_R^{\text{ind}}[n]$  is an unknown modulated signal which must be decoded in order to cancel it. This will also require accurate channel estimation and a high-resolution receiver. We note that the rate of change of ambient signals can be vastly different from the backscatter symbol rate.

It is helpful to employ a simple subsequent receive-side signal transformation,

$$y[n] := 1 + \frac{v_{\text{diff}}[n]}{Z_{RT}i_0} . \quad (9)$$

This signal has the structure  $y[n] = \Gamma[n] + v_N[n] / (Z_{RT}i_0)$ , i.e. reflection coefficient plus noise, because of (4) and (8). The transformation can be realized with phase synchronization and automatic gain control. The signal  $y[n] \in \mathbb{C}$  is henceforth considered as receive signal. We only consider BC systems whose receiver can actually realize the suggested processing steps. Implementation details and feasibility criteria are relayed to the existing literature [6].

For the noise voltage  $v_N[n] \in \mathbb{C}$  we assume a circularly-symmetric complex Gaussian distribution  $v_N[n] \sim \mathcal{CN}(0, \sigma^2)$  with variance  $\sigma^2$ . The samples are statistically independent and identically distributed (i.i.d.) for different  $n$ . This is a well-established model for thermal receiver noise [29, Sec. 2.2.4].

We have now established a simple complex-valued, discrete-time signal and noise model:

$$y[n] = \Gamma[n] + w[n], \quad w[n] \stackrel{\text{i.i.d.}}{\sim} \mathcal{CN}(0, 1/\rho) \quad (10)$$

with  $|\Gamma[n]| \leq 1 \forall n$ . The value  $\rho$  defines the signal-to-noise ratio (SNR) in accordance with [30,  $s^2$  in Tab. II],

$$\rho := \frac{|Z_{\text{RT}} i_0|^2}{\sigma^2} = \frac{|Z_{\text{RT}}|^2 |v_{\text{T}}^{\text{ind}}|^2}{4 R_{\text{T}}^2 \sigma^2}. \quad (11)$$

We will often refer to the SNR in terms of its decibel (dB) value  $10 \cdot \log_{10}(\rho)$ .

### III. ACHIEVABLE INFORMATION RATES

In accordance with typical conventions in information theory, we discard the time indexation  $[n]$  and write the signal and noise model (10) in terms of random variables (written as italic boldface symbols),

$$\mathbf{y} = \mathbf{\Gamma} + \mathbf{w}, \quad |\mathbf{\Gamma}| \leq 1, \quad \mathbf{w} \sim \mathcal{CN}(0, 1/\rho). \quad (12)$$

Throughout the paper, we assume  $\mathbf{\Gamma}$  and  $\mathbf{w}$  to be statistically independent and independently sampled for different time steps  $n$ . We do not consider any symbol decision regions or other forms of thresholding or quantization. We assume that the SNR  $\rho$  as defined in (11) is constant, which requires that both  $v_{\text{T}}^{\text{ind}}$  and  $Z_{\text{RT}}$  are constant for the duration of a load-modulated coding block. This is fulfilled in MoBC and BiBC with time-invariant or slow-fading propagation channels. It is *not* fulfilled in almost every AmBC use case, where usually  $v_{\text{T}}^{\text{ind}}$  is fluctuating rapidly due to the ambient source modulation.

The focus of this section are the achievable information rates over the channel (12) at a given SNR  $\rho$ . The mutual information  $I(\mathbf{y}; \mathbf{\Gamma})$  specifies an achievable rate [17, Cpt. 7] which is measured in bit per channel use (bpcu). From an engineering perspective, reliable communication over the channel is possible at any information rate below  $I(\mathbf{y}; \mathbf{\Gamma})$ . In particular, a suitable error-correcting code with a very large block length allows to approach  $I(\mathbf{y}; \mathbf{\Gamma})$  with an arbitrarily small block error rate [17].

As in [24, Eq. (5)], our exposition uses polar coordinates

$$\mathbf{\Gamma} = \mathbf{a} e^{j\theta}, \quad \mathbf{y} = \mathbf{b} e^{j\phi}. \quad (13)$$

We use the probability density function (PDF)  $f_{\mathbf{\Gamma}}(\Gamma)$  of  $\mathbf{\Gamma}$  with argument  $\Gamma \in \mathbb{C}$ . The PDF is necessarily zero for  $\Gamma$  outside the unit disk. Likewise, the amplitude PDFs  $f_a(a)$  and  $f_b(b)$



are zero unless  $a \in [0, 1]$  and  $b \in \mathbb{R}_{\geq 0}$ , respectively. Finally, we note that the receive-side transformations (7) and (9) do not affect the mutual information because it is invariant under smooth, uniquely invertible maps [31, Eq. (45)].

#### A. Channel Capacity, General Passive Load

It is important to understand that the mutual information  $I(\mathbf{y}; \mathbf{\Gamma})$  depends on the distribution of  $\mathbf{\Gamma}$ , i.e. on the specific transmit signaling. The channel capacity, herein denoted  $R_{\max}$ , is the supremum of  $I(\mathbf{y}; \mathbf{\Gamma})$  over all eligible distributions of  $\mathbf{\Gamma}$  (those that prohibit realizations outside the unit disk). The channel capacity is the upper limit of achievable information rates for reliable communication. [17], [29]

Consider the physical amplitude constraint  $|\mathbf{\Gamma}| \leq 1$  on the complex-valued reflection coefficient. Mathematically (but not physically),  $|\mathbf{\Gamma}|^2 \leq 1$  qualifies as a constraint on the instantaneous transmit power. A crucial consequence is that, therefore, the capacity problem of the channel in (12) is equivalent to that of a peak-power-limited quadrature Gaussian channel. The latter has been solved by Shamai & Bar-David [24]. In the following, we employ their results to solve the channel capacity problem of backscatter communication.

Foremost, we infer from [24], [32] that the capacity-achieving distribution of  $\mathbf{\Gamma} = \mathbf{a}e^{j\theta}$  has discrete amplitude  $\mathbf{a}$  and uniform independent phase  $\theta$  (DAUIP). In other words,  $f_{\mathbf{\Gamma}}(\mathbf{\Gamma})$  is supported on a finite union of concentric circles. We note that  $\mathbf{\Gamma}$  has an infinite number of mass points, which is in contrary to a statement in the BC literature [14, Sec. IV-A]. In the following, we formalize the capacity-achieving distribution by adopting statements from [24] to our notation:

- 1) The radius  $\mathbf{a}$  is chosen from a finite discrete set of radii. The set always contains the unit circle  $a_1 = 1$ :

$$\mathbf{a} \in \{a_1 = 1, a_2, \dots, a_K\}, \quad a_k \in [0, 1] \quad \forall k. \quad (14)$$

We define that the circle radii  $a_k$  are in descending order.

- 2) The radii  $a_k$  are chosen with non-uniform probabilities, denoted  $q_k$ .
- 3) The phase angle has uniform distribution  $\theta \sim \mathcal{U}(0, 2\pi)$  for any SNR  $\rho$  and is statistically independent of  $\mathbf{a}$ .
- 4) At low SNR  $\rho < 3.011$  (or rather  $\rho < 4.8$  dB), capacity is achieved by  $K = 1$  and thus  $\mathbf{a} = a_1 = 1$  with  $q_1 = 1$ . This corresponds to uniform  $\infty$ -PSK modulation.

5) The number of circles  $K$  increases with the SNR  $\rho$ .

The channel capacity  $R_{\max}$  is obtained by maximizing the mutual information with respect to the number of circles, their radii, and their probabilities:

$$\begin{aligned}
 R_{\max}(\rho) = & \max_{K, a_2, \dots, a_K, q_1, \dots, q_K} I(\mathbf{y}; \mathbf{\Gamma}) \Big|_{a \in \{1, a_2, \dots, a_K\}, \text{UIP } \theta} \\
 & \text{subject to } K \in \mathbb{N}, \quad 0 \leq a_K < \dots < a_2 < 1, \\
 & 0 < q_1, \dots, q_K \leq 1, \quad q_1 + \dots + q_K = 1.
 \end{aligned} \tag{15}$$

This optimization problem classifies as mixed-integer programming, with a variable number of parameters ( $2K$ ). Approximate  $\rho$ -thresholds for the optimality of  $K = 1, 2, 3$  are stated in [24, Tab. 1] (please note that their values are 3 dB larger because they assumed a variance of 2 for the complex-valued AWGN). The threshold  $\rho < 3.011$  for the optimality of  $K = 1$  is the numerical solution of a complicated equation [24, Eq. (45)]. The objective function  $I(\mathbf{y}; \mathbf{\Gamma})$  is also fairly complicated to compute for given parameters  $K, \{a_k\}, \{q_k\}$ ; detailed instructions are deferred to Sec. III-B.

The evolution of the channel capacity  $R_{\max}$  versus  $\rho$  is plotted in Fig. 3 (solid blue graph). It shows that high information rates in excess of 5 bpcu are possible at reasonably high SNR. This evaluation goes hand in hand with a numerical evaluation of the capacity-achieving parameters over  $\rho$ , shown in Fig. 4. It shows how new circles emerge with increasing  $\rho$ . This was implemented by iterating through a fine grid of increasing values  $\rho$  (with a 0.1 dB increment). We start at a value  $\rho < 4.8$  dB where the optimality of  $K = 1$  is formally guaranteed. After every increment of  $\rho$ , we run the following procedure. Firstly, we fix  $K$  to the previous optimal value and optimize all  $a_2, \dots, a_K$  and  $q_1, \dots, q_K$  jointly according to (15). For this purpose we use the interior-point algorithm for constrained nonlinear optimization [33] with carefully tuned stopping criteria and initialized at the preceding optimal parameter values. Secondly, we add a new circle on trial: we increment  $K$ , set the radius  $a_K = 0$ , and set  $q_K$  to some sensible nonzero initial value (we choose  $q_K = \frac{1}{100} q_1$ ). We then optimize all circle parameters with the aforementioned interior-point algorithm. If this experiment increased the mutual information by at least 1 part per million, then we keep the trial circle. Otherwise the new circle and the changes are discarded. We proceed with the next iterative increment of  $\rho$  and repeat the procedure.

It shall be noted that the choice of the numerical threshold value has a noticeable effect on the results at high-SNR. Because there, parameter fine tuning for the innermost circles causes

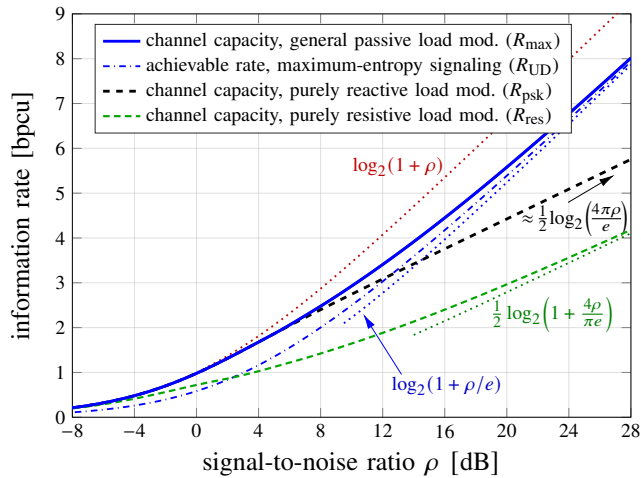


Fig. 3. Channel capacity in bit per channel use (bpcu) plotted versus SNR.

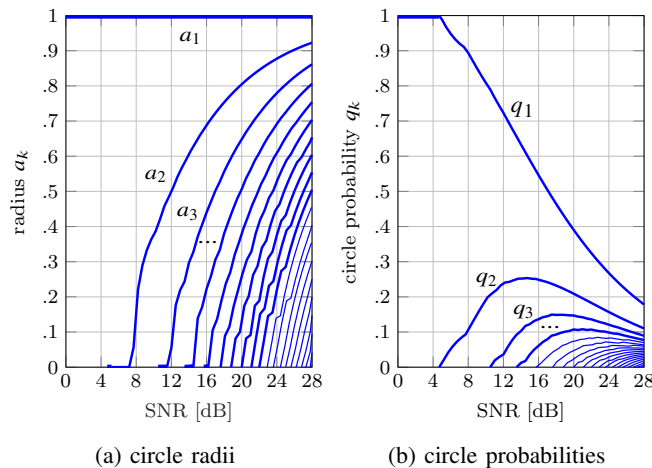


Fig. 4. Evolution of the circle radii and probabilities that describe the capacity-achieving DAUIP distribution of the load reflection coefficient  $\Gamma$ .

only tiny rate changes near the floating point accuracy. These numerical issues have also been indicated in [24] and cause the rather shaky high-SNR behavior of the smaller radii in Fig. 4a.

Fig. 5 illustrates the PDF  $f_{\Gamma}(\Gamma)$  of the capacity-achieving distribution of  $\Gamma \in \mathbb{C}$  over the complex plane, for different SNR values. This evaluation uses specific values from Fig. 4. We want to point out the following informal observations that characterize the distribution. Consider the lateral probability densities  $\lambda_k := q_k/(2\pi a_k)$  over the circumferences. At high SNR, they take similar values  $\forall k$ , so the distribution of  $\Gamma$  closely resembles a uniform distribution over the unit disk. However,  $\lambda_k$  is appreciably larger for the outmost circles: based on complementary

numerical evaluations, we conjecture that  $\lambda_2/\lambda_1 \rightarrow 2/3$  and  $\lambda_3/\lambda_1 \rightarrow 1/\sqrt{3}$  for  $\rho \rightarrow \infty$ , while for  $k > 3$  any  $\lambda_k/\lambda_1$  approaches a value slightly below  $1/\sqrt{3}$ .

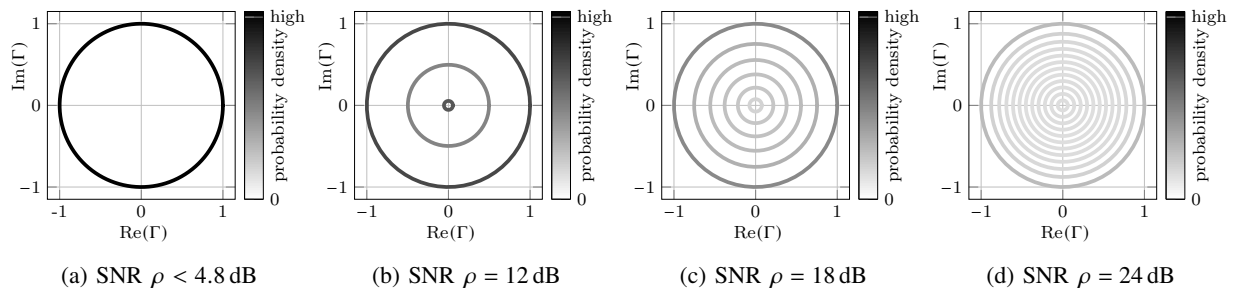


Fig. 5. Capacity-achieving distribution of the load reflection coefficient  $\Gamma \in \mathbb{C}$  for different SNR values. The color intensity actually describes the multiplier of a Dirac delta, because the probability density is either 0 or  $\infty$  as a result of the one-dimensional PDF support (the circles are infinitesimally thin).

The associated distributions of the normalized load impedance  $z = \frac{1+\Gamma}{1-\Gamma}$  could be very interesting to circuit designers. They are given and discussed in Appendix A.

### B. Calculating the Mutual Information

The additive noise channel (12) is continuous-valued and memoryless. Thus, the mutual information is over the channel is a difference of differential entropies,  $I(\mathbf{y}; \Gamma) = h(\mathbf{y}) - h(\mathbf{y}|\Gamma) = h(\mathbf{y}) - h(\mathbf{w})$ . The Gaussian noise entropy is given by  $h(\mathbf{w}) = \log_2(\frac{\pi e}{\rho})$  [29, Eq. (B.40)]. Therefore, the mutual information is

$$I(\mathbf{y}; \Gamma) = h(\mathbf{y}) + \log_2\left(\frac{\rho}{\pi e}\right). \quad (16)$$

It remains to compute the differential entropy  $h(\mathbf{y})$  of the received signal. By definition it is given by [17, Cpt. 8]

$$h(\mathbf{y}) = - \int_{\mathbb{C}} f_{\mathbf{y}}(y) \log_2(f_{\mathbf{y}}(y)) dy \quad (17)$$

which is shorthand notation for a double integral of  $\text{Re}(y)$  and  $\text{Im}(y)$  over  $\mathbb{R}^2$ .

A more specific formula can be given if  $\mathbf{y}$  has uniform independent phase (UIP). We note that  $\mathbf{y} = \Gamma + \mathbf{w}$  inherits the UIP property from  $\Gamma$  due to the circularly-symmetric  $\mathbf{w}$ . This is formalized as  $\theta, \phi \sim \mathcal{U}(0, 2\pi)$  for the polar angles in (13). Therewith, one can easily derive<sup>1</sup> the UIP-specific formula [24, Eq. (13)]

$$h(\mathbf{y}) = \log_2(2\pi) - \int_0^\infty f_b(b) \log_2\left(\frac{f_b(b)}{b}\right) db. \quad (18)$$

Used in (16) this yields the UIP-case mutual information,

$$I(\mathbf{y}; \mathbf{\Gamma}) = \log_2(2\rho/e) - \int_0^\infty f_b(b) \log_2\left(\frac{f_b(b)}{b}\right) db \quad (19)$$

$$= \log_2(2\rho/e) + h(\mathbf{b}) + \mathbb{E}[\log_2(\mathbf{b})]. \quad (20)$$

The evaluation of (19) requires the PDF of the noisy radius  $\mathbf{b} = |\mathbf{a}e^{j\theta} + \mathbf{w}|$ . It has the same statistics as  $|\mathbf{a} + \mathbf{w}|$ , i.e. a Rice distribution  $\mathbf{b}|\mathbf{a} \sim \text{Rice}(a, 1/\sqrt{2\rho})$ . With this insight, marginalization  $f_b(b) = \int_0^1 f_a(a) f_{b|a}(b|a) da$  yields the received-signal radius PDF<sup>2</sup>

$$f_b(b) = 2\rho b \int_0^1 f_a(a) e^{-\rho(b-a)^2} g(2\rho ab) da, \quad (21)$$

$$g(x) := I_0(x)e^{-x}, \quad x \in \mathbb{R}_{\geq 0}, \quad (22)$$

where  $I_0(x)$  is the modified Bessel function of the first kind. The above formulas allow to calculate the mutual information  $I(\mathbf{y}; \mathbf{\Gamma})$  for UIP  $\mathbf{\Gamma}$ , given  $f_a(a)$  and  $\rho$ . To do so, compute (19) with (21) and numerical integration. Some numerical aspects are noteworthy: In (19), a finite interval of integration  $b \in [0, 1 + 5/\sqrt{\rho}]$  suffices for accurate results. The exponentially scaled Bessel function  $g(x)$  in (21) decays rather slowly from its maximum at  $g(0) = 1$ . It should be computed directly [34] to avoid numerical problems with the rampantly increasing  $I_0(x)$ .

Consider now that  $\mathbf{\Gamma}$  has DAUIP, i.e. discrete amplitude  $\mathbf{a}$  and UIP  $\theta$ . This comprises the capacity-achieving distribution. The radius  $\mathbf{a}$  assumes a discrete distribution with a finite number of mass points; the PDF is of the form  $f_a(a) = \sum_{k=1}^K q_k \delta(a - a_k)$  where  $\delta(\cdot)$  is the Dirac delta distribution. Consequently, the integral (21) simplifies to the Rician mixture sum

$$f_b(b) = 2\rho b \sum_{k=1}^K q_k e^{-\rho(b-a_k)^2} g(2\rho a_k b). \quad (23)$$

The subsequent computation of the mutual information (19) still requires numerical integration. This way, one can compute the objective function  $I(\mathbf{y}; \mathbf{\Gamma})$  in the optimization problem (15) that determines the channel capacity.

<sup>1</sup>To derive (18), write (17) as double integral of  $b, \phi$  with Jacobian determinant  $b$ , note that  $b \cdot f_y = f_{\mathbf{b}, \phi} = \frac{1}{2\pi} f_b$  for UIP  $\Rightarrow f_y = \frac{1}{2\pi} \frac{1}{b} f_b$ . Note that the integrand is constant w.r.t.  $\phi$  and compute the trivial integral.

<sup>2</sup>Expression (21) is equivalent to [24, Eq. (11)]. A conversion from our formalism to that of Shamai and Bar-David [24] is achieved as follows. Set the peak-power to  $\rho_p := 2\rho$  and multiply (12) with  $\sqrt{\rho_p}$  to obtain a signal model  $\tilde{\mathbf{y}} = \mathbf{x} + \omega$  with  $\tilde{\mathbf{y}} = \mathbf{y}\sqrt{\rho_p}$ ,  $\mathbf{x} = \mathbf{\Gamma}\sqrt{\rho_p}$ , and  $\omega \sim \mathcal{CN}(0, 2)$ . The peak-power constraint is  $|\mathbf{x}|^2 = |\mathbf{\Gamma}|^2 \rho_p \leq \rho_p$ . The average-power constraint  $\mathbb{E}[|\mathbf{x}|^2] \leq \rho_a$  in [24, Eq. (3)] is not relevant to the backscatter problem; it is deactivated by setting  $\rho_a = \rho_p$ . In  $\mathbf{x} = \mathbf{r}e^{j\theta}$ ,  $\tilde{\mathbf{y}} = \mathbf{R}e^{j\phi}$  the polar radii fulfill  $\mathbf{a} = \mathbf{r}/\sqrt{2\rho}$ ,  $\mathbf{b} = \mathbf{R}/\sqrt{2\rho}$  and  $f_a(a) = f_r(r)\sqrt{2\rho}$ ,  $f_b(b) = f_R(R)\sqrt{2\rho}$ . With these substitutions, the equations (16),(18),(21) become [24, Eq. (4),(13),(11)]. Finally, bits are converted to nats by replacing each  $\log_2$  with  $\ln$ .

### C. Signaling Uniformly over the Unit Disk

From Fig. 5 we already made the informal observation that with increasing SNR, the capacity-achieving  $\mathbf{\Gamma} = \mathbf{a}e^{j\theta}$  more and more resembles a uniform distribution. We shall now consider such a continuous uniform distribution over the complex unit disk (henceforth referred to as UD) and study the resulting rate. The associated  $\mathbf{\Gamma}$  has UIP (but not DAUIP) and a linear radius PDF  $f_a(a) = 2a$  for  $a \in [0, 1]$ . The resulting PDF of the receive-signal radius  $\mathbf{b}$  is described by the integral (21). From a special case of [24, Eq. (33)] and a change of variables, we obtain the solution  $f_b(b) = 2b(1 - Q_1(b\sqrt{2\rho}, \sqrt{2\rho}))$  where  $Q_1(\cdot, \cdot)$  is the Marcum Q-function of order 1 [35]. The associated information rate  $R_{\text{UD}}(\rho) := h(\mathbf{y}) + \log_2(\frac{\rho}{\pi e})$  follows via (19) and numerical integration.

This signaling can be motivated intuitively. If the noise variance is very small ( $\rho \gg 1$ ), then  $\mathbf{y} = \mathbf{\Gamma} + \mathbf{w}$  is distributed similarly to  $\mathbf{\Gamma}$ . Now (16) gives  $I(\mathbf{y}; \mathbf{\Gamma}) \approx h(\mathbf{\Gamma}) + \log_2(\frac{\rho}{\pi e})$ , which is clearly maximized by maximizing  $h(\mathbf{\Gamma})$ . As argued formally in Appendix B, under the constraint  $|\mathbf{\Gamma}| \leq 1$ , a continuous uniform distribution over the complex unit disk maximizes  $h(\mathbf{\Gamma})$ .

To conclude, UD signaling allows to approach the channel capacity ( $R_{\text{UD}} \approx R_{\text{max}}$ ) at high SNR but is wasteful at low SNR. This is confirmed by the dash-dotted blue graph in Fig. 3 of  $R_{\text{UD}}$  versus  $\rho$ .

### D. Channel Capacity, Purely Reactive Load Modulation

The load could be constrained to be purely reactive for technical reasons, e.g., the load circuit should hold only capacitors and/or inductors. This is associated with a purely imaginary load impedance  $\mathbf{z} = j\mathbf{x}$  and a reflection coefficient  $\mathbf{\Gamma} = e^{j\theta}$  on the unit circle (with deterministic radius  $\mathbf{a} = 1$ ). This corresponds to PSK modulation. The interior of the unit disk is not utilized and, therefore, some rate loss is to be expected at high SNR.

From [24] we know that the mutual information is maximized by a uniform phase  $\theta \sim \mathcal{U}(0, 2\pi)$ . This is implemented into our formalism by simply setting  $K = 1$ ,  $a_1 = 1$ ,  $q_1 = 1$  in the sum (21). This yields  $\mathbf{b} \sim \text{Rice}(1, 1/\sqrt{2\rho})$  with the PDF  $f_b(b) = 2\rho b e^{-\rho(b-1)^2} g(2\rho b)$ . The channel capacity, which is denoted  $R_{\text{psk}}$  for this case, is now obtained directly with (16) because there are no free parameters left to optimize. Still, (19) must be computed with numerical integration. Very similar calculations were given in [36, Eq. (12)], [25, Eq. (14)], [24].

Following from the statements in Sec. III-A, at low SNR  $\rho < 4.8$  dB, the equality  $R_{\text{psk}} = R_{\text{max}}$  holds precisely. This is confirmed by the black dashed graph in Fig. 3, which plots the evolution

of  $R_{\text{psk}}$  versus  $\rho$ . However, we find that the high-SNR rate loss compared to  $R_{\text{max}}$  is indeed significant.

### E. Channel Capacity, Purely Resistive Load Modulation

Consider a purely resistive load with real-valued impedance  $\mathbf{z} = \mathbf{r} \in \mathbb{R}_{\geq 0}$ . Then the reflection coefficient  $\Gamma = \frac{r-1}{r+1}$  lies on the interval  $[-1, 1]$  on the real axis. Now the received imaginary part  $\text{Im}(\mathbf{y}) = \text{Im}(\Gamma + \mathbf{w}) = \text{Im}(\mathbf{w})$  bears no information about  $\Gamma$ . The mutual information is thus equivalently described by a real-valued channel  $\mathbf{y}_R = \Gamma_R + \mathbf{w}_R$  subject to  $\Gamma_R \in [-1, 1]$  and with  $\mathbf{w}_R \sim \mathcal{N}(0, 1/(2\rho))$ . The associated capacity problem was solved by Smith [23], who found that the optimal transmit distribution is discrete (i.e. a finite symbol constellation). The number of mass points, their positions and probabilities are SNR-dependent and must be found with optimization, analogous to the circle parameters in (15). The UIP-specific (15) and (18)-(23) however do not apply here.

The channel capacity is obtained by numerical maximization of  $I(\mathbf{y}_R; \Gamma_R) = \frac{1}{2} \log_2(\frac{\rho}{\pi e}) - \int_{-\infty}^{\infty} f_{\mathbf{y}_R}(y) \log_2(f_{\mathbf{y}_R}(y)) dy$  with the PDF  $f_{\mathbf{y}_R}(y) = \sqrt{\rho/\pi} \sum_{m=1}^M p_m \exp(-\rho(y-\Gamma_m)^2)$ , with respect to  $M \in \mathbb{N}$  and all free parameters  $\Gamma_m \in [-1, 1]$  and  $p_m \in [0, 1]$  subject to  $\sum_{m=1}^M p_m = 1$ . The evaluation requires numerical integration. Some parameters can be fixed because: (i) the outmost points  $\Gamma_m = \pm 1$  always occur and (ii) if  $\Gamma_m > 0$  is a mass point, then  $-\Gamma_m$  is one too and has equal probability.

The evolution of the channel capacity  $R_{\text{res}}$  versus  $\rho$  is seen at the green dashed graph in Fig. 3. At high SNR we observe a significantly decreased rate compared to all other schemes. The reason is simply that the interval  $[-1, 1] \subset \mathbb{R}$  offers less space for signaling than the unit circle or the unit disk.

### F. Insightful Bounds and Asymptotes

In the following we state various simple bounds and asymptotes which describe the rate behavior. The statements hold for nonzero, finite SNR. First of all, the general bounds

$$R_{\text{res}} < R_{\text{psk}} \leq R_{\text{max}} < \log_2(1 + \rho) < \rho \cdot \log_2(e), \quad (24)$$

$$R_{\text{max}} < 2R_{\text{res}} \quad (25)$$

apply. The bound  $\log_2(1 + \rho)$  is the well-known AWGN channel capacity with average-power constraint  $\mathbb{E}[|\Gamma|^2] \leq 1$ , which is looser than the effective  $|\Gamma|^2 \leq 1$ , cf. [14], [24]. The upper

bound  $\rho \cdot \log_2(e)$  is from log linearization. At low SNR, it is tight for all considered signaling schemes that utilize the maximum amplitude  $|\Gamma| = 1$  for every symbol:

$$\rho \ll 1 : \quad R_{\text{res}} \approx R_{\text{psk}} = R_{\text{max}} \approx \log_2(1 + \rho) \approx \rho \cdot \log_2(e). \quad (26)$$

On the other hand, in Fig. 3 we observed inferior low-SNR behavior for  $R_{\text{UD}}$  (which uses a uniform  $\mathbf{\Gamma}$  on the unit disk). This is caused by setting  $|\Gamma|$  also to values below 1, which is wasteful at low SNR where the rate is power-limited. In particular,

$$\rho \ll 1 : \quad R_{\text{UD}} \approx \frac{1}{2} R_{\text{max}} \approx \frac{\rho}{2} \cdot \log_2(e) \quad (27)$$

because 3 dB are being wasted; the mean squared amplitude is  $\mathbb{E}[\mathbf{a}^2] = \int_0^1 a^2 f_a(a) da = \frac{1}{2}$ .

The bound  $R_{\text{max}} < 2R_{\text{res}}$  is due to [24, Fig. 1 & Eq. (27)] and has an intuitive background: The disk constraint  $|\mathbf{\Gamma}|^2 = \text{Re}(\mathbf{\Gamma})^2 + \text{Im}(\mathbf{\Gamma})^2 \leq 1$  concerns both parts jointly. With a looser constraint to the bounding square  $\text{Re}(\mathbf{\Gamma}), \text{Im}(\mathbf{\Gamma}) \in [-1, 1]$ , the parts would however be uncoupled. The channel would decompose into two parallel AWGN channels, each with capacity  $R_{\text{res}}$ .

In Sec. III-C we argued that uniform signaling allows for near-capacity rates at high SNR. We shall analyze this circumstance in more detail. For the complex-valued channel  $\mathbf{y} = \mathbf{\Gamma} + \mathbf{w}$ , the two-dimensional entropy power inequality  $2^{h(\mathbf{y})} \geq 2^{h(\mathbf{\Gamma})} + 2^{h(\mathbf{w})}$  holds [37], [24, Eq. (36)]. By applying it to  $h(\mathbf{y})$  in (16) and doing basic rearrangements, we obtain

$$\log_2 \left( 1 + \frac{2^{h(\mathbf{\Gamma})}}{\pi} \cdot \frac{\rho}{e} \right) \leq I(\mathbf{y}; \mathbf{\Gamma}) \quad (28)$$

for the AWGN channel, for any distribution of  $\mathbf{\Gamma}$ . On the other hand,  $h(\mathbf{\Gamma}) \leq \log_2(\pi)$  holds and is achieved with equality through UD signaling, as argued formally in Appendix B. This yields the bounds

$$\text{in general:} \quad \log_2(1 + \rho/e) \leq R_{\text{UD}} < R_{\text{max}}, \quad (29)$$

$$\rho \gg 1 : \quad \log_2(1 + \rho/e) \approx R_{\text{UD}} \approx R_{\text{max}}. \quad (30)$$

At high SNR, this rate is 1 nats/cu = 1.44 bpcu below the famous  $\log_2(1 + \rho)$  expression. The near-optimality of a uniform distribution is intuitive to the communications engineer, e.g., in the light of high-order constellation design where equidistant symbol spacing is the natural choice.

Similarly, purely resistive load modulation can operate near channel capacity when a continuous uniform distribution is employed for the transmit signal  $\mathbf{\Gamma}_{\text{R}}$ . In detail, the real-valued AWGN channel  $\mathbf{y}_{\text{R}} = \mathbf{\Gamma}_{\text{R}} + \mathbf{w}_{\text{R}}$  fulfills the entropy power inequality  $2^{2h(\mathbf{y}_{\text{R}})} \geq 2^{2h(\mathbf{\Gamma}_{\text{R}})} + 2^{2h(\mathbf{w}_{\text{R}})}$  [37]. Now  $h(\mathbf{w}_{\text{R}}) = \frac{1}{2} \log_2(\frac{\pi e}{\rho})$  and other simple steps yield  $\frac{1}{2} \log_2(1 + \frac{\rho}{\pi e} 2^{2h(\mathbf{\Gamma}_{\text{R}})}) \leq I(\mathbf{y}_{\text{R}}; \mathbf{\Gamma}_{\text{R}})$



for the AWGN channel. Under the constraint  $\Gamma_R \in [-1, 1]$ , the bound  $h(\Gamma_R) \leq \log_2(2) = 1$  holds and is achieved with equality by  $\Gamma_R \sim \mathcal{U}(-1, 1)$ . Thus,

$$\text{in general:} \quad \frac{1}{2} \log_2 \left( 1 + \frac{4\rho}{\pi e} \right) \leq R_{\text{res}} < \frac{1}{2} \log_2(1 + 2\rho), \quad (31)$$

$$\rho \gg 1: \quad \frac{1}{2} \log_2 \left( 1 + \frac{4\rho}{\pi e} \right) \approx R_{\text{res}}. \quad (32)$$

The upper bound is the capacity of the respective real-valued AWGN channel when instead a looser constraint of average power 1 is in effect.

Regarding purely reactive load modulation, we discussed in Sec. III-D that uniform  $\infty$ -PSK is optimal and associated with a receive-amplitude distribution  $\mathbf{b} \sim \text{Rice}(1, 1/\sqrt{2\rho})$ . At high  $\rho$ , this is closely resembled by a Gaussian  $\mathbf{b} \sim \mathcal{N}(1, 1/(2\rho))$ . This allows for a simple and very accurate approximation of the channel capacity [36], [30, Table II], [24, Eq. (42)]

$$\rho \gg 1: \quad R_{\text{psk}} \approx \frac{1}{2} \log_2 \left( \frac{4\pi\rho}{e} \right). \quad (33)$$

This can easily be obtained from (20), with  $h(\mathbf{b}) \approx \frac{1}{2} \log_2(\frac{\pi e}{\rho})$  and  $\mathbb{E}[\log_2(\mathbf{b})] \approx 0$ . Comparing (33) to (32) reveals a high-SNR rate difference of  $R_{\text{psk}} - R_{\text{res}} \approx \frac{1}{2} \log_2(\pi^2) = 1.65$  bpcu. This shows a significant SNR-domain gain of  $\pi^2 \approx 10$  of reactive over resistive load modulation. This is explained by an amplitude-domain gain of  $\pi$  which arises from the circle's circumference-to-diameter ratio.

The high-SNR asymptotes (32) and (33) both exhibit a pre-log factor of  $\frac{1}{2}$ , which stems from the respective unused dimension: each scheme modulates either the resistance  $\mathbf{r}$  or the reactance  $\mathbf{x}$  of the the load impedance  $\mathbf{z} = \mathbf{r} + j\mathbf{x}$ , but not both. In terms of  $\Gamma$ , this means that the modulation utilizes either the unit-disk boundary or the contained real axis. The rate  $R_{\text{max}} \approx \log_2(1 + \rho/e)$  does not suffer this problem: the capacity-achieving scheme utilizes both dimensions of a general passive load whenever the SNR calls for that (as seen in Sec. III-A and Appendix A).

#### IV. IMPLICATIONS FOR AMBIENT BC CAPACITY

So far we have considered monostatic and bistatic BC setups, which operate under the assumption that the induced voltage phasor  $\mathbf{v}_T^{\text{ind}}$  at the tag antenna would be constant due to a dedicated RF source. Now we consider ambient BC (AmBC) where  $\mathbf{v}_T^{\text{ind}}$  is a random variable due to a modulated ambient source. In particular, we model  $\mathbf{v}_T^{\text{ind}} = \mathbf{Z}_{\text{TA}} \mathbf{i}_A$  via the mutual impedance  $\mathbf{Z}_{\text{TA}}$  from the random ambient-source antenna feed current  $\mathbf{i}_A$  to the BC tag. Other than that, we employ the same assumptions as in Sec. II. Consequently, we find that the random instantaneous

SNR of the BC link is given by  $|\mathbf{Z}_{\text{RT}}\mathbf{Z}_{\text{TA}}\mathbf{i}_A/(2R_T\sigma)|^2$ . We decompose this into a convenient product  $|\psi|^2\rho$  that is composed of the mean SNR

$$\rho := \frac{\mathbb{E}[|\mathbf{Z}_{\text{RT}}\mathbf{Z}_{\text{TA}}\mathbf{i}_A|^2]}{4R_T^2\sigma^2} \quad (34)$$

and a random variable  $\psi$  that encompasses the ambient signal modulation in  $\mathbf{i}_A$  but also potential time-varying channel fading in  $\mathbf{Z}_{\text{RT}}$  and  $\mathbf{Z}_{\text{TA}}$ . In particular,

$$\psi := \frac{\mathbf{Z}_{\text{RT}}\mathbf{Z}_{\text{TA}}\mathbf{i}_A}{\sqrt{\mathbb{E}[|\mathbf{Z}_{\text{RT}}\mathbf{Z}_{\text{TA}}\mathbf{i}_A|^2]}} \in \mathbb{C}, \quad \mathbb{E}[|\psi|^2] = 1. \quad (35)$$

We refrain from assumptions on the distribution of  $\psi$  or the correlation between  $\mathbf{Z}_{\text{RT}}$ ,  $\mathbf{Z}_{\text{TA}}$ ,  $\mathbf{i}_A$ .

We define the ratio  $N_A := T/T_A$  of the BC load-modulation symbol duration  $T$  to the coherence time  $T_A$  of  $\psi$ . Usually,  $T_A$  will be determined by the ambient-modulation symbol duration. Most BC link designs will exhibit  $N_A \gg 1$  because a large  $T$  may be necessary for sufficient noise averaging at the BC receiver and to avoid significant distortions from transients. In [14] for example,  $T$  is matched to the duration of an entire ambient OFDM symbol (e.g.,  $N_A = 64$  would be typical for an ambient WiFi signal with 64 OFDM subcarriers). The circumstance that  $\psi$  decorrelates  $N_A$  times per change of  $\Gamma[n]$  is captured by the following notation, which is analogous to [14, Eq. (38)]. For simplicity we assume  $N_A \in \mathbb{N}$  and stack the discretized temporal evolution of the random variables into the random vector  $\vec{\psi}[n] \in \mathbb{C}^{N_A}$ . As before,  $n \in \mathbb{Z}$  is the time index of the BC transmit signal  $\Gamma[n] \in \mathbb{C}$ . We obtain a vector-form signal and noise model  $\vec{y}[n] = \vec{\psi}[n]\Gamma[n] + \vec{w}[n]$  with  $\vec{y}, \vec{\psi}, \vec{w} \in \mathbb{C}^{N_A}$ . Regarding the AWGN vector  $\vec{w}[n]$ , all elements are i.i.d.  $\mathcal{CN}(0, N_A/\rho)$  whereby the factor  $N_A$  is due to the shorter time window for noise-averaging. We assume that the fluctuations in  $\vec{\psi}[n]$  are caused by a digitally modulated ambient source and that the BC receiver is able to obtain full knowledge of  $\vec{\psi}[n]$  by decoding the ambient signal and through estimating all relevant channels (cf. Sec. II). As noted in [14, Eq. (40)], the SNR-optimal strategy for the decoding of  $\Gamma[n]$  involves maximum-ratio combining, which is implemented with a projection  $y[n] := \vec{u}[n]^H \vec{y}[n]$  onto  $\vec{u}[n] := \frac{1}{\sqrt{N_A}} \vec{\psi}[n] / \|\vec{\psi}[n]\|$ . This yields the scalar model

$$y[n] = \mathbf{a}[n]\Gamma[n] + w[n], \quad \mathbf{a}[n] := \frac{1}{\sqrt{N_A}} \|\vec{\psi}[n]\|, \quad (36)$$

with  $|\Gamma[n]| \leq 1 \forall n$ ,  $w[n] \stackrel{\text{i.i.d.}}{\sim} \mathcal{CN}(0, 1/\rho)$ , and  $\mathbb{E}[|\mathbf{a}[n]|^2] = 1$ . Because of the ever-changing effect of the ambient data in  $\vec{\psi}[n]$ , it is reasonable to assume statistical independence between  $\mathbf{a}[n]$  for different  $n$ . In consequence, from the formal perspective of information theory, the

channel (36) classifies as a fast-fading AWGN channel whose coherence time equals one symbol duration (even without interleaving techniques). The capacity of this channel is given by

$$R_{\max}^{\text{AmBC}}(\rho) = \mathbb{E}_{\mathbf{a}} [R_{\max}(|\mathbf{a}|^2 \rho)] \quad (37)$$

which follows from the ergodic capacity arguments in [29, Sec. 5.4.5 & Apdx. B.7.1]. We refer to this source for the mathematical background and details on the special error-correcting codes that are required to approach capacity over a fast-fading channel. The function  $R_{\max}(\cdot)$  in (37) is the complicated expression from (15) that describes the non-ambient-case channel capacity for a constant SNR  $\rho$ . A similar observation has been made in [14, Eq. (41)]. A more detailed analytical description of  $R_{\max}^{\text{AmBC}}$  seems to be infeasible at this point. However, by Jensen's inequality, one can discern that  $R_{\max}^{\text{AmBC}}(\rho) \leq R_{\max}(\rho)$ , because of  $\mathbb{E}[|\mathbf{a}[n]|^2] = 1$  and the apparent concavity of  $R_{\max}(\rho)$ . At low SNR, the function is approximately linear, cf. (24), and thus

$$\rho \ll 1 : \quad R_{\max}^{\text{AmBC}}(\rho) \approx R_{\max}(\rho) \approx \rho \cdot \log_2(e). \quad (38)$$

Consider now the special case that the ambient rate of change is much faster than the BC symbol rate ( $N_A \gg 1$ ). Then  $|\mathbf{a}[n]|^2 = \frac{1}{N_A} \|\vec{\psi}[n]\|^2 \approx \mathbb{E}[|\psi|^2] = 1$  by the law of large numbers. Employing this in (37) yields  $R_{\max}^{\text{AmBC}}(\rho) \approx R_{\max}(\rho)$  because of  $|\mathbf{a}|^2 \approx 1$ . The effect of the ambient fluctuations is remedied entirely.

Consider now the special case of a PSK-modulated ambient source (i.e.  $\mathbf{i}_A$  has constant envelope) and that both propagation channels ( $\mathbf{Z}_{\text{RT}}, \mathbf{Z}_{\text{TA}}$ ) are time-invariant for the duration of a BC coding block. In consequence,  $|\psi|^2 = 1$ , so  $|\mathbf{a}|^2 = 1$  and  $R_{\max}^{\text{AmBC}}(\rho) = R_{\max}(\rho)$ .

Finally, consider that the coherence period of  $\mathbf{a}[n]$  is longer than the coding block length of the BC load modulation. While this is unlikely in AmBC, such conditions can certainly occur in BiBC or MoBC with slow-fading propagation channels. In this regime, the ergodic-capacity perks of the fast-fading channel are unavailable; the channel capacity is actually zero. Still, the communications performance can be meaningfully described with the outage capacity [29, Sec. 5.4.1], given by  $R_{\max}(\rho \cdot F_{|\mathbf{a}|^2}^{-1}(\epsilon))$ . It is the information rate that can be decoded with outage probability  $\epsilon$ . Thereby  $F_{|\mathbf{a}|^2}^{-1}$  is the inverse cumulative distribution function (CDF) of  $|\mathbf{a}|^2$ .

## V. TECHNICAL ASPECTS

### A. Approaching Capacity with Finite APSK Constellations

Practical modulation schemes usually avoid to sample a continuous distribution and instead use a discrete distribution (a.k.a. finite constellation, symbol alphabet). This means that  $\mathbf{\Gamma}$  is sampled

from  $\{\Gamma_1, \dots, \Gamma_M\} \subset \mathbb{C}$ ,  $|\Gamma_m| \leq 1 \forall m$ , with the probabilities  $p_m$ . The Euclidean symbol distance  $|\Gamma_m - \Gamma_n| \leq 2$  is capped by the unit-disk diameter. With an  $M$ -ary constellation, the information rate  $I(\mathbf{y}; \mathbf{\Gamma})$  will obviously be below the channel capacity  $R_{\max}$ . However, it is well known that  $R_{\max}$  can be approached with a finite constellation that resembles the capacity-achieving distribution. This has been argued rigorously in [38]–[41].

A simple observation is that the capacity-achieving distribution of a purely-reactive load (a uniform distribution over the unit circle, cf. Sec. III-D) is closely resembled by  $M$ -PSK modulation  $\Gamma_m = \exp(j2\pi \frac{m-1/2}{M})$  with  $p_m = \frac{1}{M}$ . The evaluation in Fig. 6 shows that the rate resulting from  $M = 2^4 = 16$  (black dashed graph) is very close to channel capacity (black solid graph) below an SNR threshold of about  $\rho < 15$  dB. At higher SNR, the rate is bottlenecked by the small  $M$ . This problem could be remedied entirely by increasing  $M$ .

In the case of a general passive load and high SNR, the capacity-achieving  $\mathbf{\Gamma}$  distribution over the concentric circles in Fig. 5 is naturally resembled by amplitude and phase-shift keying (APSK). This long-established scheme [30] has been used by optical [42] and satellite [43] communication systems. APSK constellation design comes with various degrees of freedom and there are different proposals for settling the details [38], [40], [44]–[46]. These nuances are however secondary, since any decent discretization of the optimal continuous distribution (for a certain SNR) will allow for a near-capacity rate. Nevertheless, we want to provide the interested reader with the following specific near-capacity APSK design for a target design-SNR  $\rho$ , tailored to the formalism at hand. First, choose the optimal number of circles  $K$  (cf. Fig. 4) and use the constellation size  $M = 4K^2$ , i.e.  $K = \sqrt{M/4}$ . Some examples are  $K = 2 \Leftrightarrow M = 16$ ,  $K = 4 \Leftrightarrow M = 64$ , and  $K = 8 \Leftrightarrow M = 256$ . As in [44], allocate  $M_k = 8(K - k) + 4$  constellation points to the  $k$ -th circle but use a constant angular spacing of  $2\pi/M_k$  on circle  $k$ . For circles with even  $k$ , introduce a rotation angle  $\pi/M_k$  to increase Euclidean distances between some symbols on neighboring circles (see Fig. 7a). Set the symbol probabilities to  $p_m = q_{k(m)}/M_{k(m)}$  based on the probability  $q_k$  of choosing the circle  $k$  that holds symbol  $\Gamma_m$ . Set the  $q_k$  and the radii  $a_k$  according to the capacity-achieving parameter set, as defined in (15) and as plotted in Fig. 4, associated with the target design-SNR.

We evaluate a 256-APSK designed for 21 dB SNR and a 64-APSK designed for 15 dB SNR. Indeed, the associated information rates (green graphs in Fig. 6) are very close to channel capacity near the respective target SNR-values. They perform significantly better than the 256-QAM benchmark, which provides worse coverage of the complex unit disk than APSK. In

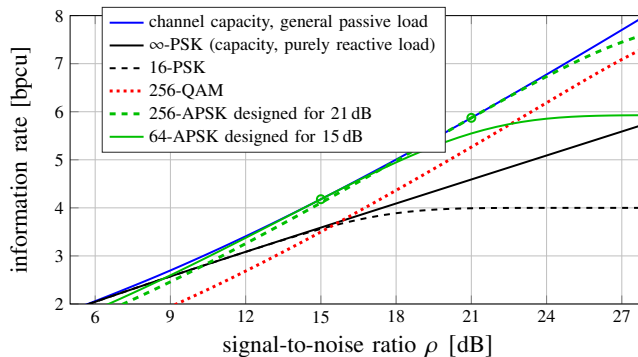


Fig. 6. Achievable information rate versus SNR for different signaling strategies and symbol constellations.

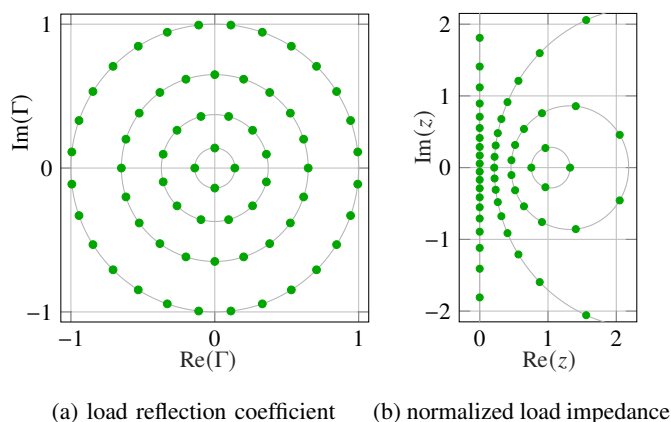


Fig. 7. 64-APSK is a suitable constellation for near-capacity backscatter information rates in the mid-SNR range.

detail, the disadvantage of a square-shaped QAM constellation is equivalent to an SNR loss of  $\frac{2}{\pi} = -1.96$  dB by the property in (39), whereby 2 is the area of a square confined in the unit disk (which itself has area  $\pi$ ).

The 64-APSK constellation design is depicted in Fig. 7a and the associated normalized load-impedance constellation  $z_m = \frac{1+\Gamma_m}{1-\Gamma_m}$  in Fig. 7b. An accurate realization with a low-cost passive load circuit is left as an interesting circuit-design challenge for future work.

Finally, we note that for a finite constellation, the source entropy  $H(\mathbf{\Gamma}) = -\sum_{m=1}^M p_m \log_2(p_m)$  caps the information rate [17]:  $I(\mathbf{y}; \mathbf{\Gamma}) \leq H(\mathbf{\Gamma}) \leq \log_2(M)$ . This comparison can reveal whether the rate is bottlenecked by a small  $M$  or whether  $M$  is unnecessarily large. A good APSK design should assert that  $H(\mathbf{\Gamma}) > R_{\max}(\rho)$  for the target design-SNR range.

In the above evaluations, we calculated the information rate  $I(\mathbf{y}; \mathbf{\Gamma})$  with (16) and (17) and numerical integration. We used the receive-signal PDF  $f_{\mathbf{y}}(y) = \frac{\rho}{\pi} \sum_{m=1}^M p_m \exp(-\rho |y - \Gamma_m|^2)$

which follows from the convolution of  $f_{\Gamma}(\Gamma) = \sum_{m=1}^M p_m \delta(\Gamma - \Gamma_m)$  with the noise PDF.

### B. High Rates with Simple Switched Loads

We consider a simple low-cost circuit for the adaptive tag load, composed of  $L + 1$  lumped elements (resistors, capacitors, inductors) in some topology. Their impedances are denoted  $Z_{\ell}$ ,  $\ell \in \{0, \dots, L\}$ . The elements  $\ell \geq 1$  are combined with individual on-off switches that allow to detach the effect of  $Z_{\ell}$  on the compound load impedance. The element  $\ell = 0$  is reactive and not switched; it establishes a near-resonant state by compensating the tag-antenna reactance  $X_T$  (like the  $-X_T$  element in Fig. 2). An example circuit is shown in Fig. 8a. It is clear that such a circuit allows for  $M = 2^L$  different load states, giving rise to an  $M$ -ary symbol constellation.

Technologically, it would be delightful if such a simple circuit could establish or approximate a near-capacity-achieving  $M$ -APSK constellation of the type discussed in Sec. V-A. Unfortunately, this is not the case: there seems to be no topology that establishes constellation points on concentric circles. Nevertheless, we shall investigate how close we can get. To do so, we maximize  $I(y; \mathbf{\Gamma})$  with respect to all component values of the topology in Fig. 8a (in omitted experiments we also evaluated other topologies, which yielded no discernible benefit) with the interior-point algorithm for gradient-based numerical optimization. In particular, we conduct a joint optimization of all component values and all symbol probabilities. The optimization is done for a design-SNR of  $\rho = 20$  dB. The symbol constellation resulting from the optimized circuit is shown in Fig. 8b in terms of reflection coefficients  $\Gamma_m$  and in Fig. 8c in terms of impedances  $z_m$ . Clearly, the constellation is far off the desired APSK constellation. The approach struggles

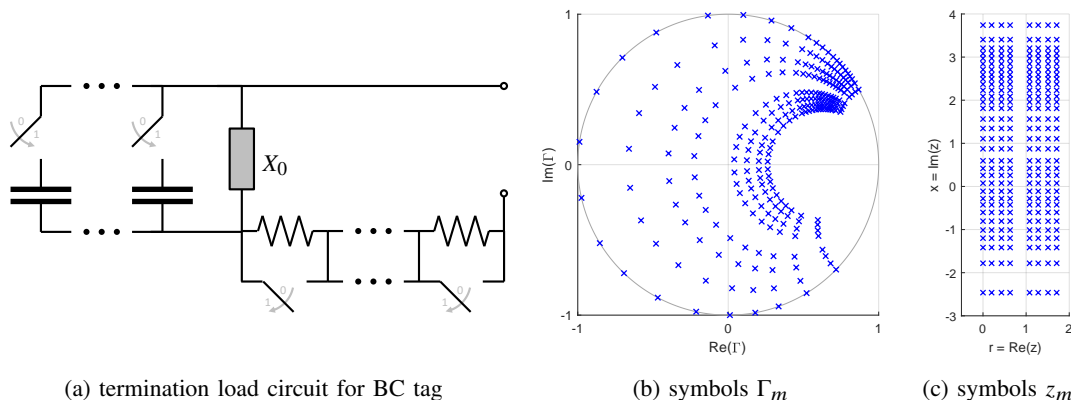


Fig. 8. A rich 8-bit symbol alphabet realized by 5 parallel switched capacitors in series with 3 switched resistors. The component values and symbol probabilities are optimized numerically for maximum achievable rate at 20 dB SNR.

with covering all regions of the unit disk with symbols  $\Gamma_m$  in a somewhat uniform fashion. We observe the following trade-off. The resistance and reactance spread is kept small to enable a decent coverage of the left, upper, and lower regions of the disk. This however prevents coverage of the entire region around  $\Gamma = 1$ , which is reached either via  $r \rightarrow \infty$ ,  $x \rightarrow \infty$ , or  $x \rightarrow -\infty$ . There is no apparent way to mitigate this trade-off.

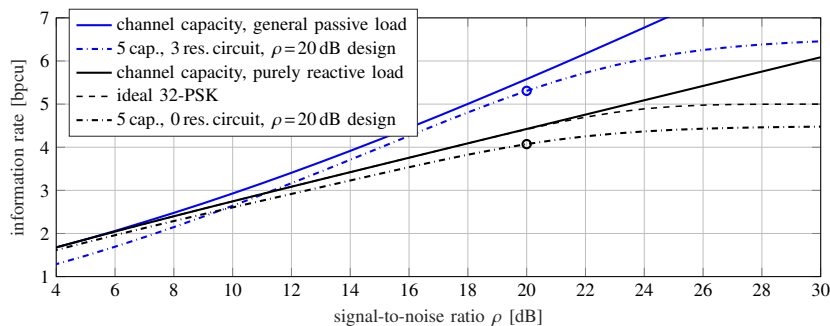


Fig. 9. Achievable rates of the simple switched circuit from Fig. 8a for the adaptive tag load, compared to benchmark cases.

Nevertheless, we find that the non-optimal constellations from such simple low-cost designs can still yield a high information rate. This is demonstrated by Fig. 9, which evaluates a general-passive circuit with  $L = 8$  switched components (5 capacitors, 3 resistors) and a purely-reactive circuit with  $L = 5$  switched capacitors (and 0 resistors), both optimized at a 20 dB target-SNR. They perform only slightly worse than the respective benchmark cases over a wide SNR range. Thereby, the optimization of the symbol probabilities is crucial, because it mitigates the non-uniform symbol spacing to a large extent. A small associated disadvantage is that the high-SNR rate limit  $H(\Gamma)$  drops below  $\log_2(M) = L$ , which is noticeable in Fig. 9.

The evaluation in Fig. 10 investigates whether the residual performance gap can be closed by adding more components to the circuit. In particular, we evaluate the achievable information rate as a function of the number of switched capacitors and resistors. Every data point is the result of a numerical optimization. The results indicate that the actual channel capacity can be approached with a reasonable number of components. Furthermore, it provides another confirmation of the importance of modulating both resistance and reactance of the load.

Finally, we want to mention that an ideal  $M$ -PSK can be realized with  $L = M/2$  switched capacitors in series. The analogous parallel design is near-optimal iff the tag antenna has a large Q-factor. The same circuits can also generate a non-ideal  $2^L$ -PSK if all switching states are utilized. The details are omitted.

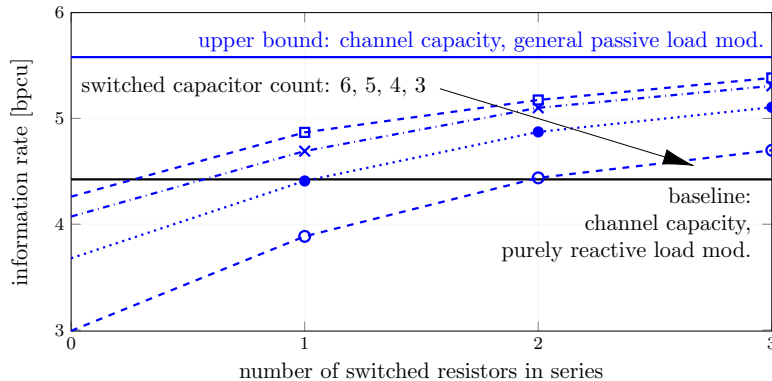


Fig. 10. Achievable information rates of the circuit from Fig. 8a for the adaptive tag load, for various resistor and capacitor counts. The rates are evaluated at 20 dB SNR and compared to channel capacity results.

### C. Effect of Value-Range Constraints on the Load

In practice it may not be possible to realize any desired reflection coefficient  $\Gamma$  on the unit disk. In the following we analyze the BC performance loss when  $\Gamma$  is restricted to a certain subset  $\mathcal{G}$  of the complex unit disk. We recall the lower bound (28) on the mutual information over a complex AWGN channel,  $\log_2(1 + \frac{\rho}{\pi e} 2^{h(\Gamma)}) \leq I(\mathbf{y}; \mathbf{\Gamma})$ . We assume that  $\mathcal{G}$  has non-empty interior and consider uniform transmit signaling  $\mathbf{\Gamma} \sim \mathcal{U}(\mathcal{G})$ . We deduct  $h(\mathbf{\Gamma}) = \log_2(\text{area}(\mathcal{G}))$  from Appendix B to obtain

$$\log_2\left(1 + \frac{\text{area}(\mathcal{G})}{\pi} \cdot \frac{\rho}{e}\right) \leq I(\mathbf{y}; \mathbf{\Gamma}). \quad (39)$$

Analogous to the arguments in Sec. III, this bound becomes tight at high SNR, in which case it constitutes an accurate approximation of the achievable rate with uniform signaling and of the channel capacity. The expression can therefore be used to assess the rate loss due to a constraint  $\Gamma \in \mathcal{G}$  with  $\text{area}(\mathcal{G}) < \pi$ . In particular, the absolute rate loss at high SNR can be quantified as  $\log_2(\pi/\text{area}(\mathcal{G}))$  bpcu.

The plots in Fig. 11 show the regions of unrealizable reflection coefficients for an exemplary inductive RFID tag. Thereby, the tag antenna coil with  $Z_T = R_T + j\omega L_T$  is loaded with an impedance  $R + \frac{1}{j\omega C}$  with adaptive resistance  $R \in \mathbb{R}_{\geq 0}$  and adaptive capacitance  $C$  with the restricted value range  $(1 - \Delta)C_{\text{res}} \leq C \leq (1 + \Delta)C_{\text{res}}$  about the resonance value  $C_{\text{res}} = 1/(\omega^2 L_T)$ . An equivalent description in our formalism from Sec. II is  $z = r + jx$  whereby the reactance  $x = x_T(1 - \frac{C_{\text{res}}}{C})$  is restricted to  $\frac{-\Delta}{1-\Delta}x_T \leq x \leq \frac{\Delta}{1+\Delta}x_T$ . Thereby  $x_T = \omega L_T/R_T$  is the coil Q-factor.



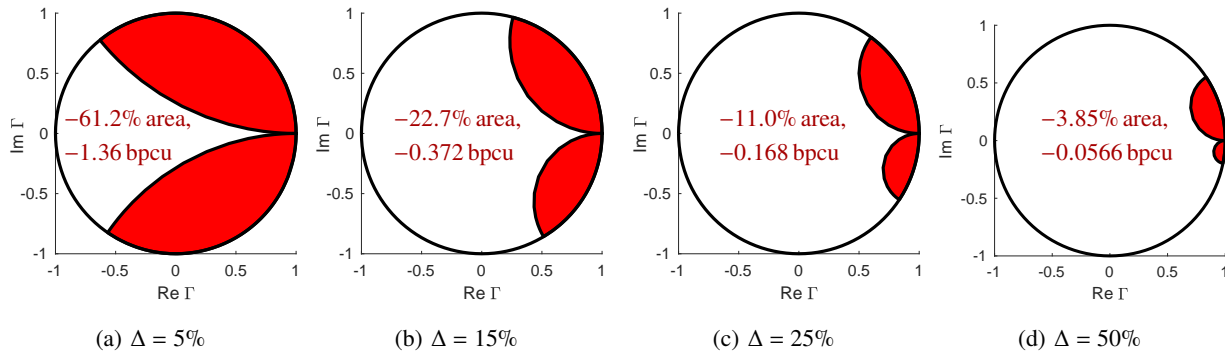


Fig. 11. Non-realizable values (red) of the load reflection coefficient due to a value-range constraint on the load reactance. This experiment assumes an inductive RFID tag. The specified bpcu value is the absolute high-SNR rate loss  $\log_2(\pi/\text{area}(\mathcal{G}))$ .

From the loss numbers in Fig. 11 we infer that load value-range constraints can have a significant effect, but mild constraints do not prohibit high data rates in BC.

In the low-SNR regime, the rate will be approximately proportional to  $d_{\max}^2$  where  $d_{\max} := \max\{|\Gamma_l - \Gamma_m| \mid \Gamma_l, \Gamma_m \in \mathcal{G}\}$  is the maximum pairwise Euclidean distance within  $\mathcal{G}$ . Since  $d_{\max} \leq 2$ , the channel capacity at low SNR can be approximated as  $(d_{\max}/2)^2 \rho \cdot \log_2(e)$  analogous to (26). In the examples in Fig. 11, the low-SNR rate loss is minimal because the entire real axis is attainable and thus  $d_{\max} = 2$ .

## VI. SUMMARY & OUTLOOK

For the first time this paper stated the channel capacity of load modulation with a freely adaptable passive impedance. The obtained insights on the capacity-achieving transmit distribution and its approximation with finite symbol alphabets and simple switched load circuits have important implications for practical high-data-rate backscatter communication systems. This applies even to the ambient backscatter case, under certain identified conditions.

Future work should incorporate the presented insights in practical BC systems in order to realize near-capacity data rates. It should also investigate the use of microwave components such as transmission lines, waveguides, ferrite phase shifters [26, Sec. 9.5] and metamaterial structures [47] for capacity-approaching load modulation.

## APPENDIX A

### IMPEDANCE STATISTICS

We characterize the distributions of the normalized load impedance  $z = \frac{1+\Gamma}{1-\Gamma}$  associated with the various different distributions of the reflection coefficient  $\Gamma$  described in Sec. III.

#### A. Capacity-Achieving Distribution, General Impedance

For values  $\Gamma = a e^{j\theta}$  on a circle with a fixed radius  $a < 1$ , the impedance values are  $z = \frac{1+a e^{j\theta}}{1-a e^{j\theta}}$ . Due to the circle preservation property of the Möbius transformation, this is another circle  $z = \frac{1+a^2}{1-a^2} + \frac{2a}{1-a^2} e^{j\beta}$  with center  $\frac{1+a^2}{1-a^2} \in \mathbb{R}$  and radius  $\frac{2a}{1-a^2} \in \mathbb{R}$ . The  $z$ -domain angle  $\beta \in [0, 2\pi)$  is a rather intricate function  $\beta(\theta) = 2 \arctan\left(\frac{\sin(\theta)}{\cos(\theta)-a}\right) - \theta$  of the  $\Gamma$ -domain angle  $\theta$ , which behaves as follows. For a small radius  $a \ll 1$ , the approximate identity  $\beta \approx \theta$  holds, so a random  $\beta$  has similar distribution as  $\theta$  (uniform). For a large radius  $a = 1 - \varepsilon$ , the angle  $\beta$  is pushed towards the value  $\pi$ , causing a concentration of probability mass near  $z = \frac{1-a}{1+a} \approx 0$ . These properties can be observed in Fig. 12 and especially in Fig. 12d. The conditional distribution  $\beta|a = a_k$  is determined by  $\theta \sim \mathcal{U}(0, 2\pi)$  and  $\beta(\theta)$ , a monotonously increasing bijective map from and to  $[0, 2\pi)$ . A change of variables yields the conditional PDF  $f_{\beta|a}(\beta|a) = f_{\theta}(\theta) \cdot \left|\frac{\partial\theta}{\partial\beta}\right| = \frac{1}{2\pi} \frac{\partial\beta}{\partial\theta} = \frac{1-2a \cos(\theta)+a^2}{2\pi(1-a^2)}$  after some rearrangements. This is an implicit formulation in terms of  $\theta$ ; an explicit one is prohibited by the unavailability of the inverse map  $\theta(\beta)$  in closed form.

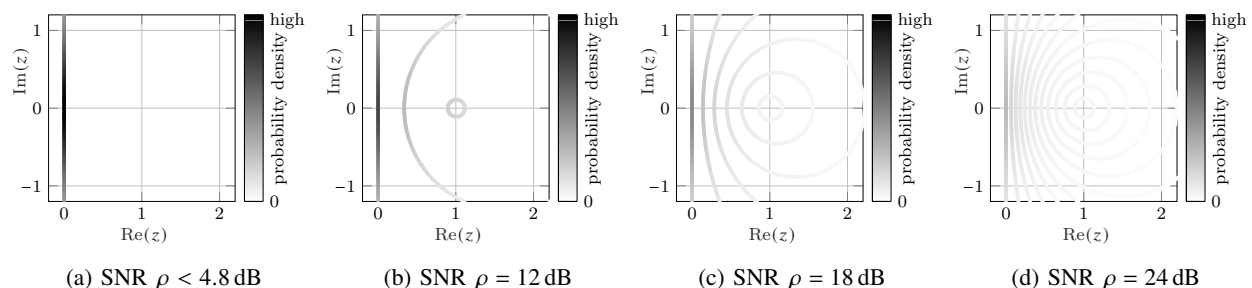


Fig. 12. Capacity-achieving distribution of the normalized load impedance  $z = \mathbf{Z}/R_T$ ,  $z \in \mathbb{C}$ , for different SNR values.

The maximum radius  $a = 1$ , associated with  $z = jx$ , will be covered in Sec. A-C.

#### B. Maximum-Entropy Transmit Signaling

In Sec. III-C we noted that a uniform distribution over the unit disk  $|\Gamma| \leq 1$  yields a near-capacity rate at high SNR. We shall describe the associated impedance distribution. For  $\Gamma = a e^{j\theta}$

we consider the joint PDF  $f_{a,\theta}(a, \theta) = f_a(a) f_\theta(\theta) = 2a \frac{1}{2\pi}$ . We write  $z = r + jx = \frac{1+ae^{j\theta}}{1-ae^{j\theta}}$  in vector form  $[r, x] = [1 - a^2, 2a \sin(\theta)] / (1 + a^2 + 2a \cos(\theta))$ . A two-dimensional change of variables yields the joint PDF  $f_z(z) = f_{r,x}(r, x) = \frac{a}{\pi} \cdot |\det(\frac{\partial[r,x]}{\partial[a,\theta]})|^{-1}$ . A detailed expansion of the  $2 \times 2$  Jacobian matrix  $\frac{\partial[r,x]}{\partial[a,\theta]}$  is omitted. To evaluate the expression use  $a = |\frac{z-1}{z+1}|$  and  $\theta = \arg(\frac{z-1}{z+1})$ . An evaluation of the PDF  $f_z(z)$  is given by the intensity plot in Fig. 13. It exhibits a concentration of probability mass near  $z = 0$  but also heavy tails in both resistance and reactance, which are hard to discern here. We observe that the PDF is a continuous approximation of capacity-achieving PDFs at high SNR, such as those in Fig. 12c and 12d.

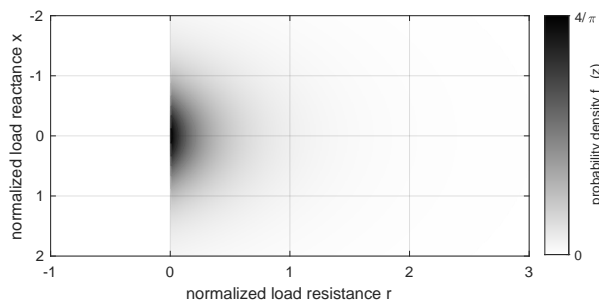


Fig. 13. Distribution of the normalized load impedance  $z \in \mathbb{C}$  associated with maximum-entropy transmit signaling, i.e. with a uniform reflection coefficient  $\Gamma$  over the unit disk.

### C. Purely Reactive Load Modulation

We found that  $\Gamma = e^{j\theta}$  with  $\theta \sim \mathcal{U}(0, 2\pi)$  achieves channel capacity for a purely reactive load (Sec. III-D) or for the low-SNR case of a general passive load (Sec. III-A). To determine the associated impedance statistics, we note that  $z = \frac{1+e^{j\theta}}{1-e^{j\theta}} = jx$  is on the imaginary axis, with the normalized load reactance  $x = \cot(\theta/2)$ . By a change of variables we find that  $x$  has the PDF  $f_x(x) = \frac{1}{\pi(1+x^2)}$ ,  $x \in \mathbb{R}$ , which is a standard Cauchy distribution (a.k.a. Lorentz distribution). This Cauchy PDF can be seen along the imaginary axes of all plots in Fig. 12. It has significant tails, i.e. large positive and negative  $x$ -values are chosen with significant probability.

### D. Purely Resistive Load Modulation

Consider a real-valued  $\Gamma = \Gamma_R \in [-1, 1]$ , associated with the resistance  $z = r = \frac{1+\Gamma}{1-\Gamma} \in \mathbb{R}^+$ . In Sec. III-E we noted that the capacity-achieving distribution is discrete, with mass points  $\Gamma_m$  and resistances  $r_m = \frac{1+\Gamma_m}{1-\Gamma_m}$ . If instead real-valued maximum-entropy signaling  $\Gamma \sim \mathcal{U}(-1, 1)$  is used to approach capacity at high SNR, then  $r$  is distributed according to the PDF  $f_r(r) = \frac{1}{(1+r)^2}$

and CDF  $F_r(r) = \frac{r}{1+r}$  with  $r \in \mathbb{R}^+$ . This is an instance of various established distributions: standard Beta prime  $r \sim \beta'(1, 1)$ , Pareto type II  $r \sim \text{Lomax}(1, 1)$ , and log-logistic  $r \sim \text{LL}(1, 1)$ . It exhibits a heavy tail but also a tendency towards small  $r$ , i.e. towards resonance.

## APPENDIX B

### MAXIMUM ENTROPY OF A VARIABLE CONSTRAINED TO A FINITE SUBAREA OF THE COMPLEX PLANE

Consider a continuous complex-valued random variable  $\mathbf{x}$  whose realizations are constrained to a compact set  $\mathcal{A} \subset \mathbb{C}$  with non-empty interior, i.e.  $0 < \text{area}(\mathcal{A}) < \infty$  with  $\text{area}(\mathcal{A}) := \int_{\mathcal{A}} dx$ . Then the differential entropy is upper-bounded by  $h(\mathbf{x}) \leq \log_2(\text{area}(\mathcal{A}))$ . Equality holds for a uniform distribution  $\mathbf{x} \sim \mathcal{U}(\mathcal{A})$ .

*Proof Sketch:* The optimality of  $\mathbf{x} \sim \mathcal{U}(\mathcal{A})$  follows from an  $\mathbb{R}^2$  description of  $\text{Re}(\mathbf{x}), \text{Im}(\mathbf{x})$  and applying [17, Thm. 12.1.1] which dictates that, in the absence of further constraints, the entropy-maximizing PDF must be constant inside the support set, i.e.  $f_{\mathbf{x}}(x) = 1/\text{area}(\mathcal{A})$ . Then  $h(\mathbf{x}) := - \int_{\mathcal{A}} f_{\mathbf{x}}(x) \log_2(f_{\mathbf{x}}(x)) dx = - \log_2(1/\text{area}(\mathcal{A})) \int_{\mathcal{A}} f_{\mathbf{x}}(x) dx = \log_2(\text{area}(\mathcal{A}))$ .

## REFERENCES

- [1] G. Dumphart, J. Sager, and A. Wittneben, "The channel capacity of general complex-valued load modulation for backscatter communication," in *Proc. IEEE Wireless Commun. Netw. Conf.* IEEE, 2022, pp. 2661–2666.
- [2] N. Van Huynh, D. T. Hoang, X. Lu, D. Niyato, P. Wang, and D. I. Kim, "Ambient backscatter communications: A contemporary survey," *IEEE Commun. Surveys Tuts.*, vol. 20, no. 4, pp. 2889–2922, 2018.
- [3] G. Wang, F. Gao, R. Fan, and C. Tellambura, "Ambient backscatter communication systems: Detection and performance analysis," *IEEE Trans. Commun.*, vol. 64, no. 11, pp. 4836–4846, 2016.
- [4] V. Chawla and D. S. Ha, "An overview of passive RFID," *IEEE Commun. Mag.*, vol. 45, no. 9, pp. 11–17, 2007.
- [5] K. Finkenzerler, *RFID Handbook*, 3rd ed. John Wiley & Sons, 2010.
- [6] R. Duan, X. Wang, H. Yigitler, M. U. Sheikh, R. Jantti, and Z. Han, "Ambient backscatter communications for future ultra-low-power machine type communications: Challenges, solutions, opportunities, and future research trends," *IEEE Commun. Mag.*, vol. 58, no. 2, pp. 42–47, 2020.
- [7] H. Zhao, Y. Shuang, M. Wei, T. J. Cui, P. d. Hougne, and L. Li, "Metasurface-assisted massive backscatter wireless communication with commodity Wi-Fi signals," *Nature Commun.*, vol. 11, no. 1, pp. 1–10, 2020.
- [8] P.-H. P. Wang, C. Zhang, H. Yang, D. Bharadia, and P. P. Mercier, "A 28 $\mu$ W IoT tag that can communicate with commodity WiFi transceivers via a single-side-band QPSK backscatter communication technique," in *IEEE Int. Solid-State Circuits Conf.* IEEE, 2020, pp. 312–314.
- [9] G. Yang, Y.-C. Liang, R. Zhang, and Y. Pei, "Modulation in the air: Backscatter communication over ambient OFDM carrier," *IEEE Trans. Commun.*, vol. 66, no. 3, pp. 1219–1233, 2017.
- [10] T. Y. Kim and D. I. Kim, "Optimum MCS for high-throughput long-range ambient backscatter communication networks," in *IEEE Int. Workshop SPAWC*, 2017, pp. 1–5.

- [11] Y. Peng, L. Shangguan, Y. Hu, Y. Qian, X. Lin, X. Chen, D. Fang, and K. Jamieson, "PLoRa: a passive long-range data network from ambient LoRa transmissions," in *Conf. ACM Special Interest Group Data Commun.*, 2018, pp. 147–160.
- [12] M. Hesar, A. Najafi, and S. Gollakota, "Netscatter: Enabling large-scale backscatter networks," in *USENIX Symp. Netw. Syst. Design Implement. (NSDI 19)*, 2019, pp. 271–284.
- [13] G. Brooker and J. Gomez, "Lev Termen's Great Seal Bug analyzed," *IEEE Aerosp. Electron. Syst. Mag.*, vol. 28, no. 11, pp. 4–11, 2013.
- [14] D. Darsena, G. Gelli, and F. Verde, "Modeling and performance analysis of wireless networks with ambient backscatter devices," *IEEE Trans. Commun.*, vol. 65, no. 4, pp. 1797–1814, 2017.
- [15] J. Kimionis, A. Georgiadis, S. N. Daskalakis, and M. M. Tentzeris, "A printed millimetre-wave modulator and antenna array for backscatter communications at gigabit data rates," *Nature Electron.*, pp. 1–8, 2021.
- [16] C. E. Shannon, "A mathematical theory of communication," *Bell System Technical Journal*, vol. 27, no. 3, pp. 379–423, Jul. 1948.
- [17] T. M. Cover and J. A. Thomas, *Elements of Information Theory*. John Wiley & Sons, 2006.
- [18] W. Zhao, G. Wang, R. Fan, L.-S. Fan, and S. Atapattu, "Ambient backscatter communication systems: Capacity and outage performance analysis," *IEEE Access*, vol. 6, pp. 22 695–22 704, 2018.
- [19] C. Liu, Z. Wei, D. W. K. Ng, J. Yuan, and Y.-C. Liang, "Deep transfer learning for signal detection in ambient backscatter communications," *IEEE Trans. Wireless Commun.*, vol. 20, no. 3, pp. 1624–1638, 2020.
- [20] F. Fuschini, C. Piersanti, F. Paolazzi, and G. Falciasecca, "On the efficiency of load modulation in RFID systems operating in real environment," *IEEE Antennas Wireless Propag. Lett.*, vol. 7, pp. 243–246, 2008.
- [21] A. I. Barbero, E. Rosnes, G. Yang, and O. Ytrehus, "Near-field passive RFID communication: Channel model and code design," *IEEE Trans. Commun.*, vol. 62, no. 5, pp. 1716–1727, 2014.
- [22] D. T. Hoang, D. Niyato, P. Wang, D. I. Kim, and Z. Han, "Ambient backscatter: A new approach to improve network performance for RF-powered cognitive radio networks," *IEEE Trans. Commun.*, vol. 65, no. 9, pp. 3659–3674, 2017.
- [23] J. G. Smith, "The information capacity of amplitude-and variance-constrained scalar Gaussian channels," *Information and Control*, vol. 18, no. 3, pp. 203–219, 1971.
- [24] S. Shamai and I. Bar-David, "The capacity of average and peak-power-limited quadrature Gaussian channels," *IEEE Trans. Inf. Theory*, vol. 41, no. 4, pp. 1060–1071, 1995.
- [25] R. Duan, R. Jäntti, H. Yigitler, and K. Ruttik, "On the achievable rate of bistatic modulated rescatter systems," *IEEE Trans. Veh. Tech.*, vol. 66, no. 10, pp. 9609–9613, 2017.
- [26] D. Pozar, *Microwave Engineering*. Wiley, 2004.
- [27] W. K. Kahn and H. Kurss, "Minimum-scattering antennas," *IEEE Trans. Antennas Propag.*, vol. 13, no. 5, pp. 671–675, 1965.
- [28] G. Dumphart, "Magneto-inductive communication and localization: Fundamental limits with arbitrary node arrangements," Ph.D. dissertation, ETH Zürich, Dept. IT & EE, 2020, Available online: <https://www.research-collection.ethz.ch/handle/20.500.11850/445440>.
- [29] D. Tse and P. Viswanath, *Fundamentals of Wireless Communication*. Cambridge University Press, 2005.
- [30] N. M. Blachman, "A comparison of the informational capacities of amplitude-and phase-modulation communication systems," *Proc. IRE*, vol. 41, no. 6, pp. 748–759, 1953.
- [31] A. Kraskov, H. Stögbauer, and P. Grassberger, "Estimating mutual information," *Physical review E*, vol. 69, no. 6, p. 066138, 2004.
- [32] T. H. Chan, S. Hranilovic, and F. R. Kschischang, "Capacity-achieving probability measure for conditionally Gaussian channels with bounded inputs," *IEEE Trans. Inf. Theory*, vol. 51, no. 6, pp. 2073–2088, 2005.

- [33] MathWorks Inc. (2022) Constrained nonlinear optimization algorithms - fmincon interior point algorithm. [Online]. Available: <https://mathworks.com/help/optim/ug/constrained-nonlinear-optimization-algorithms.html>
- [34] ——. (2022) Modified Bessel function of first kind – Calculate exponentially scaled modified Bessel functions. [Online]. Available: <https://ch.mathworks.com/help/matlab/ref/besseli.html>
- [35] ——. (2022) Generalized Marcum Q-function. [Online]. Available: <https://ch.mathworks.com/help/signal/ref/marcumq.html>
- [36] A. D. Wyner, “Bounds on communication with polyphase coding,” *Bell System Technical Journal*, vol. 45, no. 4, pp. 523–559, 1966.
- [37] N. Blachman, “The convolution inequality for entropy powers,” *IEEE Trans. Inf. Theory*, vol. 11, no. 2, pp. 267–271, 1965.
- [38] W. Huleihel, Z. Goldfeld, T. Koch, M. Madiman, and M. Médard, “Design of discrete constellations for peak-power-limited complex Gaussian channels,” in *IEEE Int. Symp. Inf. Theory*. IEEE, 2018, pp. 556–560.
- [39] J. Huang and S. P. Meyn, “Characterization and computation of optimal distributions for channel coding,” *IEEE Trans. Inf. Theory*, vol. 51, no. 7, pp. 2336–2351, 2005.
- [40] H. Méric, “Approaching the Gaussian channel capacity with APSK constellations,” *IEEE Commun. Lett.*, vol. 19, no. 7, pp. 1125–1128, 2015.
- [41] Y. Wu and S. Verdú, “The impact of constellation cardinality on Gaussian channel capacity,” in *Proc. 48th Allerton Conf. Commun., Control, Computing*. IEEE, 2010, pp. 620–628.
- [42] D. Zou, C. Lin, and I. B. Djordjevic, “FPGA-based LDPC-coded APSK for optical communication systems,” *Optics Express*, vol. 25, no. 4, pp. 3133–3142, 2017.
- [43] R. De Gaudenzi, A. G. i Fabregas, and A. Martinez, “Performance analysis of turbo-coded APSK modulations over nonlinear satellite channels,” *IEEE Trans. Wireless Commun.*, vol. 5, no. 9, pp. 2396–2407, 2006.
- [44] F. Kayhan, “QAM to circular isomorphic constellations,” in *Advanced Sat. Multimedia Sys. Conf. and Signal Proc. for Space Commun. Workshop*. IEEE, 2016, pp. 1–5.
- [45] A. Ž. Jovanović, I. B. Djordjevic, Z. H. Perić, and S. A. Vlajkov, “Circularly symmetric companding quantization-inspired hybrid constellation shaping for APSK modulation to increase power efficiency in Gaussian-noise-limited channel,” *IEEE Access*, vol. 9, pp. 4072–4083, 2020.
- [46] D. Yoda and H. Ochiai, “Decision region optimization and metric-based compensation of memoryless nonlinearity for APSK systems,” *IEEE Trans. Broadcast.*, vol. 64, no. 2, pp. 281–292, 2018.
- [47] H. Yang, X. Cao, F. Yang, J. Gao, S. Xu, M. Li, X. Chen, Y. Zhao, Y. Zheng, and S. Li, “A programmable metasurface with dynamic polarization, scattering and focusing control,” *Scientific reports*, vol. 6, no. 1, pp. 1–11, 2016.